INTERNATIONAL JOURNAL FOR NUMERICAL METHODS IN FLUIDS
Int. J. Numer. Meth. Fluids 2009; **61**:144–164
Published online 4 November 2008 in Wiley InterScience (www.interscience.wiley.com). DOI: 10.1002/fld.1949

A nodal integral method for quadrilateral elements

Erfan G. Nezami[1], Suneet Singh[3], Nahil Sobh[2] and Rizwan-uddin[3,*,†]

[1]*Landau Associates, 130 2nd Ave South, Edmonds, WA 98020, U.S.A.*
[2]*Civil and Environmental Engineering and National Center for Supercomputing Applications, University of Illinois at Urbana-Champaign, 205 North Mathews Ave Urbana, IL 61801, U.S.A.*
[3]*Department of Nuclear, Plasma and Radiological Engineering, University of Illinois at Urbana-Champaign, 216 Talbot Lab, 104 S. Wright St., Urbana, IL 61801, U.S.A.*

SUMMARY

Nodal integral methods (NIMs) have been developed and successfully used to numerically solve several problems in science and engineering. The fact that accurate solutions can be obtained on relatively coarse mesh sizes, makes NIMs a powerful numerical scheme to solve partial differential equations. However, transverse integration procedure, a step required in the NIMs, limits its applications to brick-like cells, and thus hinders its application to complex geometries. To fully exploit the potential of this powerful approach, abovementioned limitation is relaxed in this work by first using algebraic transformation to map the arbitrarily shaped quadrilaterals, used to mesh the arbitrarily shaped domain, into rectangles. The governing equations are also transformed. The transformed equations are then solved using the standard NIM. The scheme is developed for the Poisson equation as well as for the time-dependent convection–diffusion equation. The approach developed here is validated by solving several benchmark problems. Results show that the NIM coupled with an algebraic transformation retains the coarse mesh properties of the original NIM. Copyright © 2008 John Wiley & Sons, Ltd.

Received 9 December 2007; Revised 5 August 2008; Accepted 10 September 2008

KEY WORDS: nodal integral method; convection–diffusion; algebraic transformation; Poisson equation; irregular-shaped elements; coarse mesh methods

1. INTRODUCTION

The nuclear industry generally uses production codes based on nodal methods for solving neutron diffusion and transport equations. An early review of nodal methods, developed and used by the nuclear industry, is given by Lawrence [1]. Nodal schemes are developed by approximately satisfying the governing differential equations on finite size brick-like elements that are obtained by discretizing the space of independent variables.

*Correspondence to: Rizwan-uddin, Department of Nuclear, Plasma and Radiological Engineering, University of Illinois at Urbana-Champaign, 216 Talbot Lab, 104 S. Wright St., Urbana, IL 61801, U.S.A.
†E-mail: rizwan@uiuc.edu

Due to their higher accuracy, various approaches based on nodal methods have been used in other branches of science and engineering to develop efficient numerical schemes [2–4]. Hennart [5] discusses nodal methods as a general class of computational schemes. Nodal integral methods (NIMs), a subclass of nodal methods, have been developed for the steady-state [6] and time-dependent [7] Navier–Stokes equations. NIM was developed for the steady-state Boussinesq equations for natural convection, and for several steady-state incompressible flow problems [8]. Esser and Witt [9] applied a nodal scheme to the two-dimensional (2D), vorticity-stream function formulation of the Navier–Stokes equations. NIM scheme for solving the time-dependent heat conduction problem was developed by Wilson *et al.* [7]. Michael *et al.* [10] developed a second- and a third-order NIM for the convection–diffusion equation. Although highly innovative, those early applications of nodal methods for the Navier–Stokes equations did not take full advantage of the potential that the nodal approach offers. An improved method has recently been developed to solve the incompressible Navier–Stokes equations. This modified nodal integral method was first developed for 2D time-dependent problems [11], and then extended for 3D time-dependent flows as well [12].

Although the NIM yields accurate results with coarse meshes, the full exploitation of its efficiency is limited due to its applicability only to the meshes, which are constituted by rectangular (or in case of 3D, cuboidal) cells. This limitation comes from the transverse integration procedure required in the development of the NIM schemes. One approach used to overcome this limitation is to couple the NIM-based schemes with other schemes (e.g. finite element, finite analytic, etc.). This approach has been used by Toreja and Rizwan-uddin [13] for fluid flow problems, and by Gu and Rizwan-uddin [14] for neutron diffusion equation. In this paper a method is developed to circumvent this limitation using a different approach.

In the current approach, the domain of computation is divided into arbitrary four-sided cells (referred to as four-node elements subsequently) and then each element is mapped into a square element of unit dimension through algebraic transformation. The scheme is developed to solve the resulting transformed equation. The algebraic transformations are commonly used for the schemes based on the finite element method [15–17]. The sensitivity of the solution to the element distortion has been studied by various authors in this context [18–22]. Ooi *et al.* [23] and Rajendran *et al.* [24] have given methods to enhance mesh distortion tolerance of the isoparametric elements. Similar studies have been carried out in the present work.

2. FORMULATION

In the following formulation, x and y are the axes in the global coordinate system while s and t are axes in the local coordinate system. The unknown function in the partial differential equations (PDEs) is T, and τ represents the time.

The space is decomposed into arbitrary four-node elements, such as that shown in Figure 1. The global coordinates are transformed into local (element) coordinates as described in the following sections.

2.1. Coordinate transform

Consider a generic four-node 2D element specified in the spatial domain $\hat{\Omega}$ characterized by global coordinate axes x and y. The objective is to transform the coordinate of the irregular domain $\hat{\Omega}$

DOI: 10.1002/fld

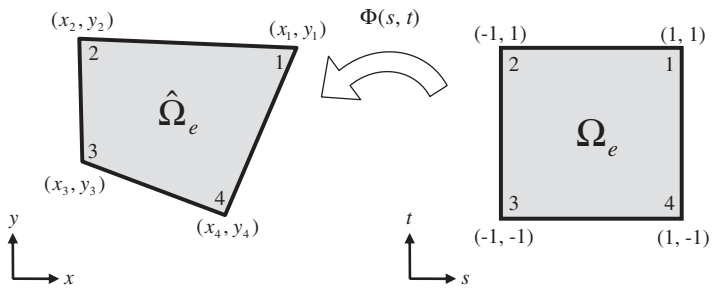

Figure 1. Coordinate transformation.

to a square domain Ω, which is characterized by the local coordinate axes s and t, as shown in Figure 1. This type of element mapping is used extensively in the finite element method during the numerical evaluation of integrals and in the representation of curved boundaries [15]. The details of this mapping are discussed next.

Let (x_i, y_i) be the coordinates of the ith corner of $\hat{\Omega}_e$. Then, the following equation defines a continuous mapping $\Phi(s,t)$ from Ω_e to $\hat{\Omega}_e$ (see also Appendix A):

$$\begin{aligned} x &= \frac{(1+s)(1+t)}{4}x_1+\frac{(1-s)(1+t)}{4}x_2+\frac{(1-s)(1-t)}{4}x_3+\frac{(1+s)(1-t)}{4}x_4 \\ y &= \frac{(1+s)(1+t)}{4}y_1+\frac{(1-s)(1+t)}{4}y_2+\frac{(1-s)(1-t)}{4}y_3+\frac{(1+s)(1-t)}{4}y_4 \end{aligned} \tag{1}$$

For this mapping, a function $\hat{T}(x,y)$ defined over $\hat{\Omega}_e$ can be transformed into a function $T(s,t)$ defined over Ω_e by substituting for x and y from the above equation.

$$T(s,t)=\hat{T}(x(s,t), y(s,t)) \tag{2}$$

Furthermore, if the inverse of $\Phi(s,t)$ exists then one can transform functions defined over (s,t) into functions defined over (x,y) as follows:

$$\hat{T}(x,y)=T(s(x,y), t(x,y)) \tag{3}$$

Differentiating Equation (3) with respect to x and y results in

$$\begin{aligned} \hat{T}_x &= T_s \cdot s_x + T_t \cdot t_x \\ \hat{T}_y &= T_s \cdot s_y + T_t \cdot t_y \end{aligned} \tag{4}$$

and

$$\begin{aligned} \hat{T}_{xx} &= T_s \cdot s_{xx} + T_t \cdot t_{xx} + s_x(T_{ss} \cdot s_x + T_{st} \cdot t_x) + t_x(T_{ts} \cdot s_x + T_{tt} \cdot t_x) \\ \hat{T}_{yy} &= T_s \cdot s_{yy} + T_t \cdot t_{yy} + s_y(T_{ss} \cdot s_y + T_{st} \cdot t_y) + t_y(T_{ts} \cdot s_y + T_{tt} \cdot t_y) \\ \hat{T}_{xy} &= T_s \cdot s_{xy} + T_t \cdot t_{xy} + s_x(T_{ss} \cdot s_y + T_{st} \cdot t_y) + t_x(T_{ts} \cdot s_y + T_{tt} \cdot t_y) \end{aligned} \tag{5}$$

DOI: 10.1002/fld

where s_x is the derivative of dependent variable s with respect to the variable x. The other subscripts also define the derivatives with respect to corresponding variables.

Consider a PDE, represented by the linear second-order differential operator Γ operating on $\hat{T}$ in the spatial domain $\hat{\Omega}$

$$\hat{\Gamma}(\hat{T}) = F_1\hat{T}_x + F_2\hat{T}_y + F_3\hat{T}_{xx} + F_4\hat{T}_{yy} = \hat{p}(x, y) \tag{6}$$

where $F_i = F_i(x, y)$. Equations (3)–(5) map this PDE into another linear second-order PDE in the spatial domain Ω as follows:

$$\Gamma(T) = f_1T_s + f_2T_t + f_3T_{ss} + f_4T_{tt} + f_5T_{st} = p(s, t) \tag{7}$$

where $f_n = f_n(s, t), -1 \leqslant s, t \leqslant 1, n = 1\text{–}5$, so that instead of solving Equation (6) in the global domain $\hat{\Omega}$, one can seek the solution of Equation (7) in the local domain Ω.

In general, for a space decomposition in the global domain $\hat{\Omega}$, each element is mapped into a regular element in the local domain. As a result each element may have a different mapping depending on its geometry. For that reason, the values of coefficients f_i may not be same for all the elements in the domain. In other words, the resulting PDE (Equation (7)) may have a different form for each element. In the following sections, NIM formulations for two special cases of Equation (6), namely, Poisson's equation and convection–diffusion equation are discussed in detail.

2.2. Formulation for 2D Poisson equation

Consider the four-node irregular element (i, j) in the global spatial decomposition $\hat{\Omega}$. The Poisson equation in this domain is given as follows:

$$\frac{\partial^2\hat{T}}{\partial x^2} + \frac{\partial^2\hat{T}}{\partial y^2} = \hat{p}(x, y) \tag{8}$$

The corresponding equation in local coordinate system (for each element) will be:

$$f_1\frac{\partial T}{\partial s} + f_2\frac{\partial T}{\partial t} + f_3\frac{\partial^2 T}{\partial s^2} + f_4\frac{\partial^2 T}{\partial t^2} + f_5\frac{\partial^2 T}{\partial s\partial t} = p(s, t) \tag{9}$$

where

$$\begin{aligned} f_1(s, t) &= s_{xx} + s_{yy} \\ f_2(s, t) &= t_{xx} + t_{yy} \\ f_3(s, t) &= s_x^2 + s_y^2 \\ f_4(s, t) &= t_x^2 + t_y^2 \\ f_5(s, t) &= 2(s_x \cdot t_x + s_y \cdot t_y) \end{aligned} \tag{10}$$

It should be emphasized that Equation (9) and the subsequent equations are valid only over an element (i, j). Also, for all the equations in this section a subscript (i, j) is implied, unless a different

DOI: 10.1002/fld

subscript is explicitly used. Equation (9) is operated by $\frac{1}{2}\int_{-1}^{1} \mathrm{d}s$ and $\frac{1}{2}\int_{-1}^{1} \mathrm{d}t$ independently, leading to two second-order ordinary differential equations as follows:

$$\begin{aligned} f_{20}\bar{T}_t^s(t)+f_{40}\bar{T}_{tt}^s(t) &= \bar{S}_1^s(t)=\frac{1}{2}\int_{-1}^{1}(p-f_1T_s-f_3T_{ss}-f_5T_{st})\,\mathrm{d}s \\ f_{10}\bar{T}_s^t(s)+f_{30}\bar{T}_{ss}^t(s) &= \bar{S}_2^t(s)=\frac{1}{2}\int_{-1}^{1}(p-f_2T_t-f_4T_{tt}-f_5T_{st})\,\mathrm{d}t \end{aligned} \tag{11}$$

where transverse-integrated functions are defined as

$$\begin{aligned} \bar{T}^s &= \frac{1}{2}\int_{-1}^{1} T(s,t)\,\mathrm{d}s \\ \bar{T}^t &= \frac{1}{2}\int_{-1}^{1} T(s,t)\,\mathrm{d}t \end{aligned} \tag{12}$$

f_{n0} is obtained by averaging f_n over the element, i.e.

$$f_{n0}=\frac{1}{4}\int_{-1}^{1}\int_{-1}^{1} f_n\,\mathrm{d}s\,\mathrm{d}t, \quad n=1,\ldots,5 \tag{13}$$

It should be noted that to arrive at Equation (11), two successive approximations are used. The first approximation (shown here only for the first term on the left-hand side of the first ODE in Equation (11)) is

$$\frac{1}{2}\int_{-1}^{1} f_2(s,t)\frac{\partial T}{\partial s}\,\mathrm{d}s \approx \frac{1}{2}\int_{-1}^{1} f_2(s,t)\,\mathrm{d}s\int_{-1}^{1}\frac{\partial T}{\partial s}\,\mathrm{d}s \tag{14}$$

Similar approximations are used for other terms. The second approximation is as follows:

$$\frac{1}{2}\int_{-1}^{1} f_n(s,t)\,\mathrm{d}s \approx \frac{1}{4}\int_{-1}^{1}\int_{-1}^{1} f_n\,\mathrm{d}s\,\mathrm{d}t, \quad n=1,\ldots,5 \tag{15}$$

These approximations are commonly used in the NIM [10–12] and have been shown to be consistent with the order of the numerical scheme [10]. It is also pointed out that the terms in Equation (11), for which the integration and differential operators do not commute, are kept on the right-hand side of the equation as the pseudo-source terms [10–12].

The unknown inhomogeneous terms on the right-hand side of Equation (11) are expanded in Legendre polynomials and truncated at the zeroth order to replace $\bar{S}_1^s(t)$ and $\bar{S}_2^t(s)$ with constants $\bar{S}_1^{s0}$ and $\bar{S}_2^{t0}$, respectively.

It should be noted from Equation (10) that f_3 and f_4 are always non-zero resulting in non-zero values of f_{30} and f_{40} in Equation (11). The coefficients f_{10} and f_{20}, however, may become zero depending on the geometry of the original element. The analytical solutions of Equation (11) are different for zero and non-zero values of f_{10} and f_{20}. For the first ODE in Equation (11) the

DOI: 10.1002/fld

solution is:
if $f_{20}=0$

$$\bar{T}^s(t)=\frac{\bar{S}_1^{s0}}{2f_{40}}(t^2-1)+\frac{\bar{T}^s(1)-\bar{T}^s(-1)}{2}t+\frac{\bar{T}^s(1)+\bar{T}^s(-1)}{2}$$

if $f_{20}\neq 0$

$$\bar{T}^s(t)=\frac{\bar{S}_1^{s0}}{f_{20}}(t-1)+\frac{2\bar{S}_1^{s0}}{f_{20}}\frac{\exp(-f_{24}(t-1))-1}{\exp(2f_{24})-1}+\bar{T}^s(1)\frac{\exp(2f_{24})-\exp(-f_{24}(t-1))}{\exp(2f_{24})-1}$$

$$+\bar{T}^s(-1)\frac{\exp(-f_{24}(t-1))-1}{\exp(2f_{24})-1} \tag{16}$$

where $f_{24}=f_{20}/f_{40}$. Similar equations can be written for the second ODE in Equation (11).

Equation (16) and its counterpart in s direction are written for each element in terms of unknown pseudo-source terms $\bar{S}_1^{s0}$ and $\bar{S}_2^{t0}$; and unknown edge-averaged values $\bar{T}^s(1)$, $\bar{T}^s(-1)$, $\bar{T}^t(1)$ and $\bar{T}^t(-1)$. Therefore, six constraints per element are needed to complete the set of equations.

To obtain the first constraint the transformed PDE (Equation (9)) is operated by $\frac{1}{4}\int_{-1}^{1}\int_{-1}^{1}\mathrm{d}s\,\mathrm{d}t$. Then, invoking the definitions of pseudo-source terms (Equation (11)) yields (also see Appendix B)

$$\bar{S}_1^{s0}+\bar{S}_2^{t0}=\bar{p}^{st}=\frac{1}{4}\int_{-1}^{1}\int_{-1}^{1}p(s,t)\,\mathrm{d}s\,\mathrm{d}t \tag{17}$$

The uniqueness of integral over the element results in the second constraint (see Appendix C):

$$\frac{1}{2}\int_{-1}^{1}\bar{T}^s\,\mathrm{d}t=\frac{1}{2}\int_{-1}^{1}\bar{T}^t\,\mathrm{d}s \tag{18}$$

The other four constrains are obtained by imposing the continuity of the function and its derivatives on the edges shared between the two adjacent elements.

Consider two adjacent elements (i, j) and $(i+1, j)$; then, the continuity of function indicates that

$$T_{i,j}^s(1)=T_{i+1,j}^s(-1) \tag{19}$$

Another set of equations enforce the continuity of the gradient of the function in the direction normal to the edge at the midpoint (x_0, y_0) of the common edge:

$$\mathbf{m}\cdot\nabla\hat{T}_{i,j}|_{(x_0,y_0)}=\mathbf{m}\cdot\nabla\hat{T}_{i+1,j}|_{(x_0,y_0)} \tag{20}$$

where $\mathbf{m}=(m_x, m_y)$ is normal to the common edge between two adjacent elements. The objective is to write both sides of this equation in terms of the unknown pseudo-source terms and the

DOI: 10.1002/fld

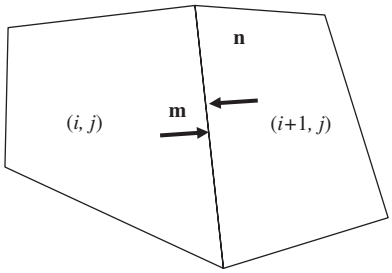

Figure 2. Compatibility criterion at the edge between two adjacent elements.

edge-averaged values of the corresponding element. Consider an element such as (i, j) shown in Figure 2.

$$\nabla \hat{T}_{i,j} = \nabla T_{i,j} \cdot J(x, y) \tag{21}$$

The term $\nabla T_{i,j} = (\partial T_{i,j}/\partial s, \partial T_{i,j}/\partial t)$, evaluated at midpoints of each edge, is approximated in terms of edge-averaged values of the element (i, j), as described below:

$$\begin{aligned} \frac{\partial T_{i,j}}{\partial s}(s,t) &= \frac{\partial \bar{T}^t_{i,j}}{\partial s}(s) \\ \frac{\partial T_{i,j}}{\partial t}(s,t) &= \frac{\partial \bar{T}^s_{i,j}}{\partial t}(t) \end{aligned} \tag{22}$$

Similarly, continuity of the temperature and heat flux can be applied at the interface of the (i, j) and $(i, j+1)$ element. The process is carried out in each element resulting in a complete set of algebraic equations for the unknowns in the global domain. The solution of these equations yields edge-averaged temperature for all the edges in the domain. Note that NIM yields edge-averaged values instead of the point values [10–12].

2.3. NIM formulation for 2D steady-state and time-dependent convection–diffusion equation

The time-dependent convection–diffusion equation in the original coordinate system is

$$\frac{\partial \hat{T}}{\partial \tau} + u\frac{\partial \hat{T}}{\partial x} + v\frac{\partial \hat{T}}{\partial y} = \mu\left(\frac{\partial^2 \hat{T}}{\partial x^2} + \frac{\partial^2 \hat{T}}{\partial y^2}\right) - \hat{p}(x, y, \tau) \tag{23}$$

where $\hat{T}$ is the temperature, u and v are velocities in the x and y directions, respectively, p is the source/sink term and μ is the diffusion coefficient. The time axis is discretized with a constant time interval $2\Delta\tau$. The discretization in space is same as the that in the steady-state case. The PDE obtained by the coordinate transformation (in each element) is

$$f_1\frac{\partial T}{\partial s} + f_2\frac{\partial T}{\partial t} + f_3\frac{\partial^2 T}{\partial s^2} + f_4\frac{\partial^2 T}{\partial t^2} + f_5\frac{\partial^2 T}{\partial s \partial t} = p(s, t, \tau) + \frac{\partial T}{\partial \tau} \tag{24}$$

DOI: 10.1002/fld

where

$$\begin{aligned} f_1 &= \mu(s_{xx}+s_{yy})-u\cdot s_x-v\cdot s_y \\ f_2 &= \mu(t_{xx}+t_{yy})-u\cdot t_x-v\cdot t_y \\ f_3(s,t) &= \mu(s_x^2+s_y^2) \\ f_4(s,t) &= \mu(t_x^2+t_y^2) \\ f_5(s,t) &= 2\mu(s_x\cdot t_x+s_y\cdot t_y) \end{aligned} \tag{25}$$

It is to be noted from Equation (24) that the transformed steady-state convection–diffusion equation will be same as the transformed Poisson equation (Equation (11)), except for the modification in the f terms as shown in Equation (25). Hence, NIM developed for the Poisson equation can be used for the steady-state convection–diffusion equation with appropriate modification in the f_{n0} ($n=1$–5) terms.

The basic methodology used here for the time-dependent convection–diffusion equation with quadrilateral elements has been previously developed for the same equation with rectangular elements [10]. For this equation, the transverse-integrated variables are defined as:

$$\begin{aligned} \bar{T}^{st} &= \frac{1}{4}\int_{-1}^{1}\int_{-1}^{1} T\,\mathrm{d}s\,\mathrm{d}t \\ \bar{T}^{s\tau} &= \frac{1}{4\Delta\tau}\int_{-1}^{1}\int_{\Delta\tau}^{\Delta\tau} T\,\mathrm{d}\tau\,\mathrm{d}s \\ \bar{T}^{t\tau} &= \frac{1}{4\Delta\tau}\int_{-1}^{1}\int_{\Delta\tau}^{\Delta\tau} T\,\mathrm{d}\tau\,\mathrm{d}t \end{aligned} \tag{26}$$

Applying the NIM methodology leads to three ODE equations, two of which are similar to Equation (11). The set of ODEs is as follows:

$$\begin{aligned} f_{20}\bar{T}_t^{s\tau}(t)+f_{40}\bar{T}_{tt}^{s\tau}(t) &= \bar{S}_1^{s\tau}(t)=\frac{1}{2\Delta\tau}\int_{-\Delta\tau}^{\Delta\tau}\int_{-1}^{1}(p-f_1T_s-f_3T_{ss}-f_5T_{st})\,\mathrm{d}s\,\mathrm{d}\tau \\ f_{10}\bar{T}_s^{t\tau}(s)+f_{30}\bar{T}_{ss}^{t\tau}(s) &= \bar{S}_2^{t\tau}(s)=\frac{1}{2\Delta\tau}\int_{-\Delta\tau}^{\Delta\tau}\int_{-1}^{1}(p-f_2T_t-f_4T_{tt}-f_5T_{st})\,\mathrm{d}t\,\mathrm{d}\tau \\ \bar{T}_\tau^{st}(\tau) &= \bar{S}_3^{st}(\tau)=\frac{1}{4}\int_{-1}^{1}\int_{-1}^{1}(f_1T_s+f_2T_t+f_3T_{ss}+f_4T_{tt}+f_5T_{st}-p)\,\mathrm{d}s\,\mathrm{d}t \end{aligned} \tag{27}$$

The pseudo-source terms are expanded in Legendre polynomials and truncated at zeroth order. This expansion and truncation allows one to solve the ODEs analytically.

The first two ODEs in Equation (27) have the same solutions as the ODEs in Equation (11). The third ODE has the following solution:

$$\bar{T}^{st}(\tau)=(\tau+\Delta\tau)\bar{S}_3^{st0}+\bar{T}^{st}(-\Delta\tau) \tag{28}$$

DOI: 10.1002/fld

Three restrictions on pseudo-source terms (similar to Equations (17) and (18)) are:

$$\bar{S}_1^{s\tau 0}+\bar{S}_2^{t\tau 0}-\bar{S}_3^{st0}=\bar{p}^{st\tau}=\frac{1}{8\Delta\tau}\int_{\Delta\tau}^{-\Delta\tau}\int_{-1}^{1}\int_{-1}^{1}p(s,t,\tau)\,\mathrm{d}s\,\mathrm{d}t\,\mathrm{d}\tau$$
$$\frac{1}{2}\int_{-1}^{1}\bar{T}^{s\tau}\,\mathrm{d}t=\frac{1}{2}\int_{-1}^{1}\bar{T}^{t\tau}\,\mathrm{d}s=\frac{1}{2\Delta\tau}\int_{-\Delta\tau}^{\Delta\tau}\bar{T}^{st}\,\mathrm{d}\tau \tag{29}$$

In addition to spatial continuity equations (which are same as Equations (19) and (20)), continuity in time is also considered as follows:

$$\bar{T}^{st}_{i,j,n-1}(\Delta\tau)=\bar{T}^{st}_{i,j,n}(-\Delta\tau) \tag{30}$$

The above equation results in a scheme for marching in time.

3. NUMERICAL RESULTS AND DISCUSSION

It is clear from the formulation that the transformed equations for the Poisson equation and the convection–diffusion equation are similar to each other. Therefore, results are presented only for the convection–diffusion equation.

3.1. Steady-state convection–diffusion equation

In this section, a steady-state convection–diffusion problem, similar to what is presented in Toreja and Rizwan-uddin [13], is discussed. The objective of the problem is to calculate the temperature distribution T in the flow between two parallel plates with a constant heat flux, q, imposed on both plates (Figure 3). The flow velocity is given by

$$u(y)=\frac{3}{2}\bar{u}\left(1-\left(\frac{y}{h}\right)^2\right) \tag{31}$$

where $\bar{u}$ is the mean velocity in the channel and h is shown in the figure. The exact solution in the channel is given as [25]

$$T(x,y)=\left(\frac{qh}{k}\right)\left\{\left(\frac{3}{4}\right)\left(\frac{y}{h}\right)^2\left(1-\frac{y^2}{6h^2}\right)+\left(\frac{4}{Pe}\right)\left(\frac{x}{h}\right)\right\} \tag{32}$$

where k is the fluid thermal conductivity and Pe is the Peclet number.

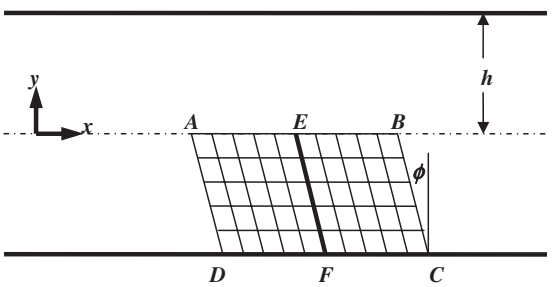

Figure 3. Schematic for steady-state diffusion problem in a channel; horizontal distortion.

DOI: 10.1002/fld

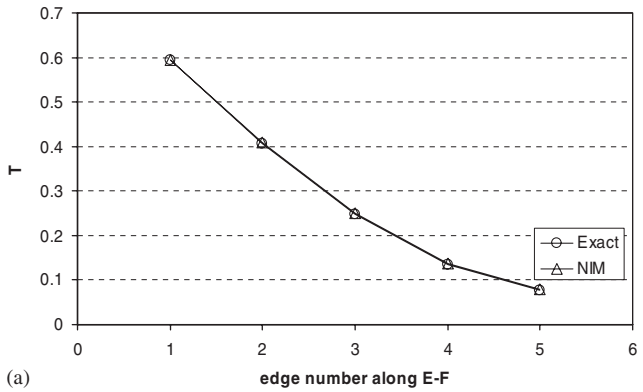

(a)

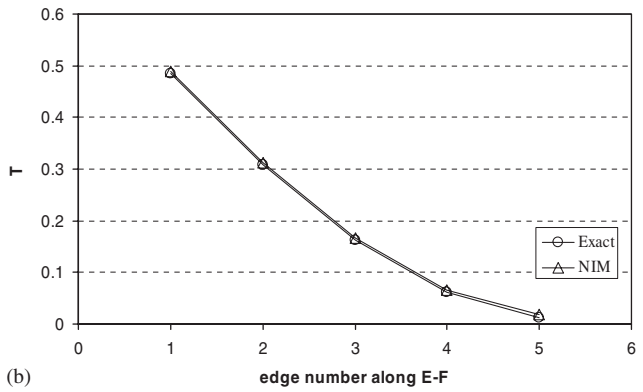

(b)

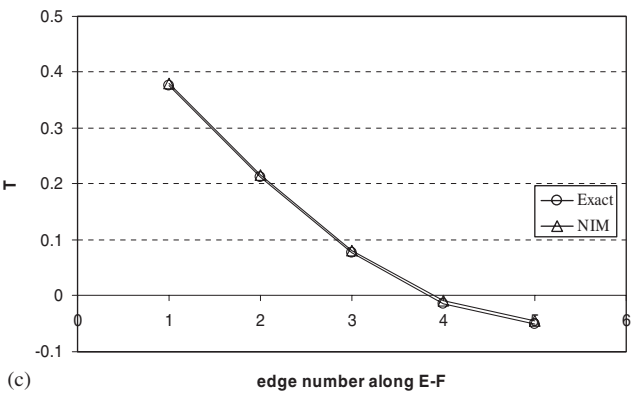

(c)

Figure 4. Effect of horizontal distortion of the mesh. The edge numbers are counted from E to F: (a) $\tan\phi = 0$; (b) $\tan\phi = 1$; and (c) $\tan\phi = 2$.

The current implementation of NIM is employed to calculate the temperature distribution T inside the channel over the parallelogram domain shown in Figure 3. In this figure, $D(1, -2.5)$ and $C(5, -2.5)$, and points A and B are located on the x-axis. The domain is divided into a 5

DOI: 10.1002/fld

by 10 mesh. The calculations are carried out with $qh/k=1$, $Pe=70$ and $h=2.5$. The boundary conditions are defined along the external edges according to Equation (32).

Various degrees of distortion in the mesh are achieved by 'sliding' edge AB along the x-axis. The horizontal distortion of the mesh is identified by the angle ϕ, measured between the edge BC and the vertical axis. Three different values of ϕ, corresponding to $\tan\phi=0$, $\tan\phi=1$ and $\tan\phi=2$, were used. The temperature T is evaluated at the center of the edges along the line EF (where E and F bisect edges AB and CD, respectively). Figure 4 plots the results for each value of ϕ, along with the exact solution. It is observed that the calculated NIM values closely follow the exact solution. The distortion of the mesh introduces some errors in the calculated values of T; however, the relative error never exceeds 2%.

In order to further observe the effect of distortion, the same mesh is distorted vertically by keeping points $A(1,0)$ and $D(1,-2.5)$ fixed and moving the edge BC vertically toward the positive-y direction (Figure 5). ϕ, the angle between edge CD and the horizontal line in Figure 5, measures the vertical distortion of the mesh. Three different meshes corresponding to $\tan\phi=0$, $\tan\phi=0.5$ and $\tan\phi=1$ are used and for each mesh the temperature T along the line EF is calculated. The plots of the temperature are shown in Figure 6.

3.2. Time-dependent convection–diffusion equation

The first problem chosen for the time-dependent problem is similar to the problem discussed in the context of steady-state convection–diffusion equation. The difference from the earlier problem is that instead of a constant heat flux a time-dependent source term is applied in the equation, which is given as [25]:

$$Ac\exp(-ct)f(x,y) \tag{33}$$

where

$$f(x,y)=\left(\frac{3}{4}\right)\left(\frac{y}{h}\right)^2\left(1-\frac{y^2}{6h^2}\right)+\left(\frac{4}{Pe}\right)\left(\frac{x}{h}\right) \tag{34}$$

This problem is solved by Toreja and Rizwan-uddin [13] with hybrid NIM. Figure 7 shows the computational domain as well as a generic 4×4 grid used for the solution. Similar grids with larger number of elements are also used.

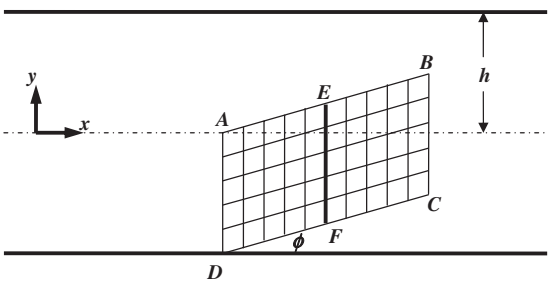

Figure 5. Schematic for steady-state convection–diffusion problem in a channel; vertical distortion.

DOI: 10.1002/fld

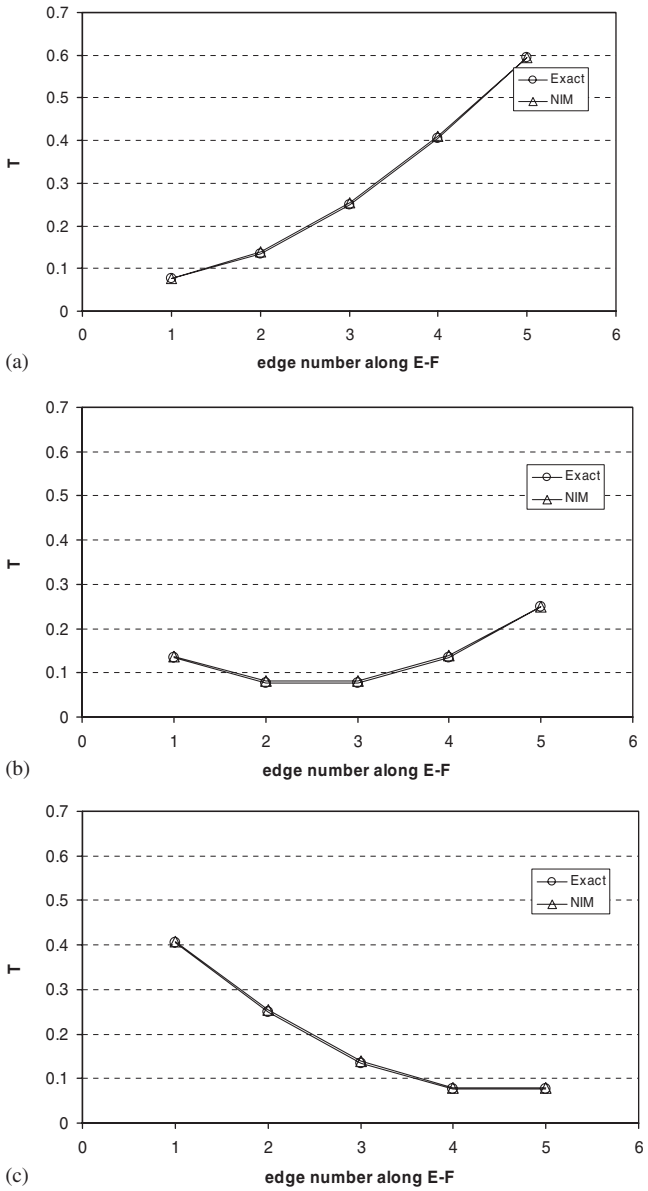

Figure 6. Effect of vertical distortion of the mesh. The edge numbers are counted from E to F: (a) $\tan\phi = 0$; (b) $\tan\phi = 0.5$; and (c) $\tan\phi = 1$.

The results for three Peclet numbers for which results are presented here are 0.7, 70 and 700. The plots of the solution with a 4×4 grid are given in Figure 8 and those with 6×6 grid are given in Figure 9.

DOI: 10.1002/fld

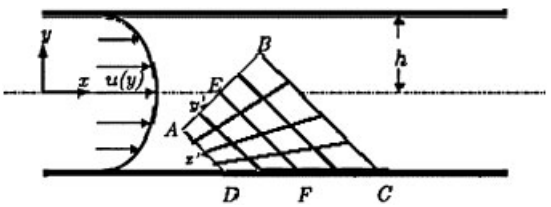

Figure 7. Schematic for time-dependent convection–diffusion problem in a channel.

The second problem chosen for application of the scheme is the convection of a Gaussian hump in a rotating velocity field. The schematic of the problem is shown in Figure 10. The problem has been previously solved by using hybrid NIM by Toreja and Rizwan-uddin [13]. The convection is large compared with the diffusion in the equation. The diffusion coefficient μ is 10^{-5} and the flow field is given as:

$$\mathbf{V}=\begin{pmatrix}2-y\\ x-2\end{pmatrix} \tag{35}$$

with the initial temperature as follows:

$$T(x,y,t=0)=\exp\left(-\frac{(x-x_0)^2}{2\sigma^2}-\frac{(y-y_0)^2}{2\sigma^2}\right) \tag{36}$$

For the present simulation $\sigma=0.15$ and $(x_0, y_0)=(2.86, 2.86)$. The problem is solved in an annulus of inner radius 0.5 and outer radius 2 with the center of the annulus at $(x, y)=(2, 2)$.

Figure 11 shows the generic grid used for the problem. Similar grids are used for different numbers of total elements. Figures 12(a) and (b) shows the results with total number of elements 3600 and 4800, respectively. Numerical diffusion in the scheme can be seen in the figure as broadening of the Gaussian distribution as well as reduction in the peak value of the Gaussian. The peak value of the Gaussian, after one rotation, reduces from 1 to 0.977 and 0.986, in the case of 3600 elements 4800 elements, respectively. It should be noted that numerical diffusion is not large and decreases with increasing number of elements. Moreover, all the commonly used numerical schemes suffer from the numerical diffusion and the present scheme is no exception.

4. CONCLUSIONS

The NIM scheme is developed for a domain consisting of arbitrarily shaped quadrilaterals. The algebraic transform is used to transform these quadrilaterals to squares. The scheme is developed for the resulting transformed equation. The distortion of the nodes from the rectangles results in increase in the error. This behavior is similar to finite volume- or finite element-based schemes.

DOI: 10.1002/fld

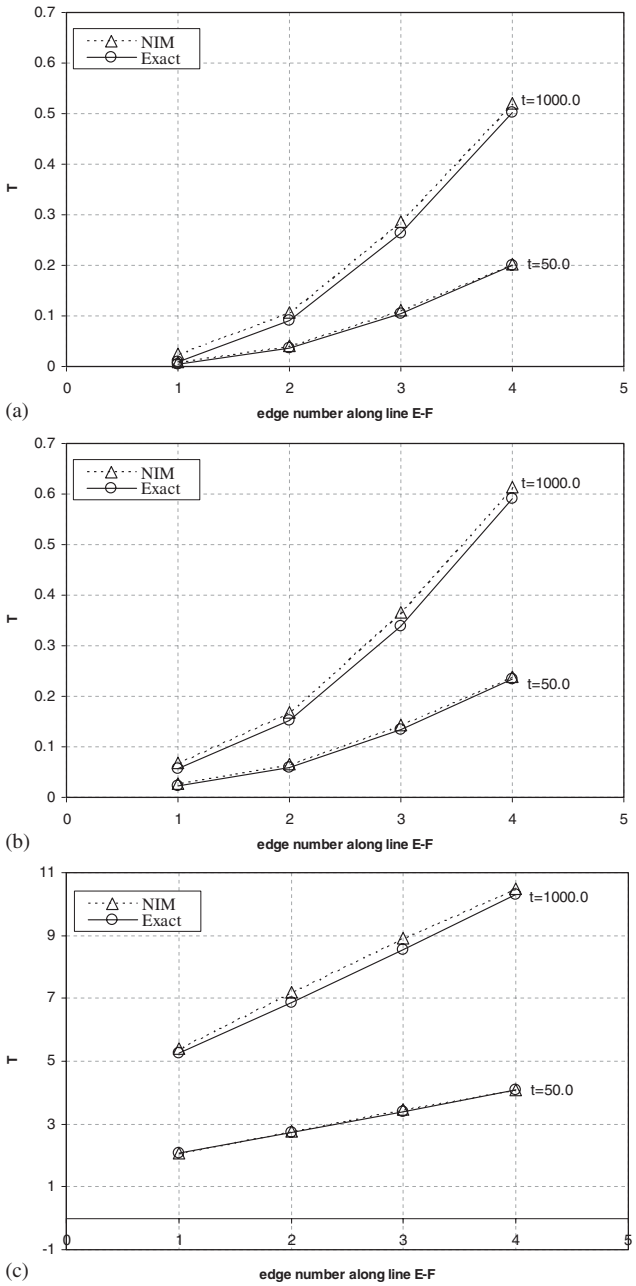

Figure 8. Calculated values for the time-dependent convection–diffusion problem along the EF with 4×4 grid. The edge numbers are counted from E to F: (a) $Pe = 700$; (b) $Pe = 70$; and (c) $Pe = 0.7$.

DOI: 10.1002/fld

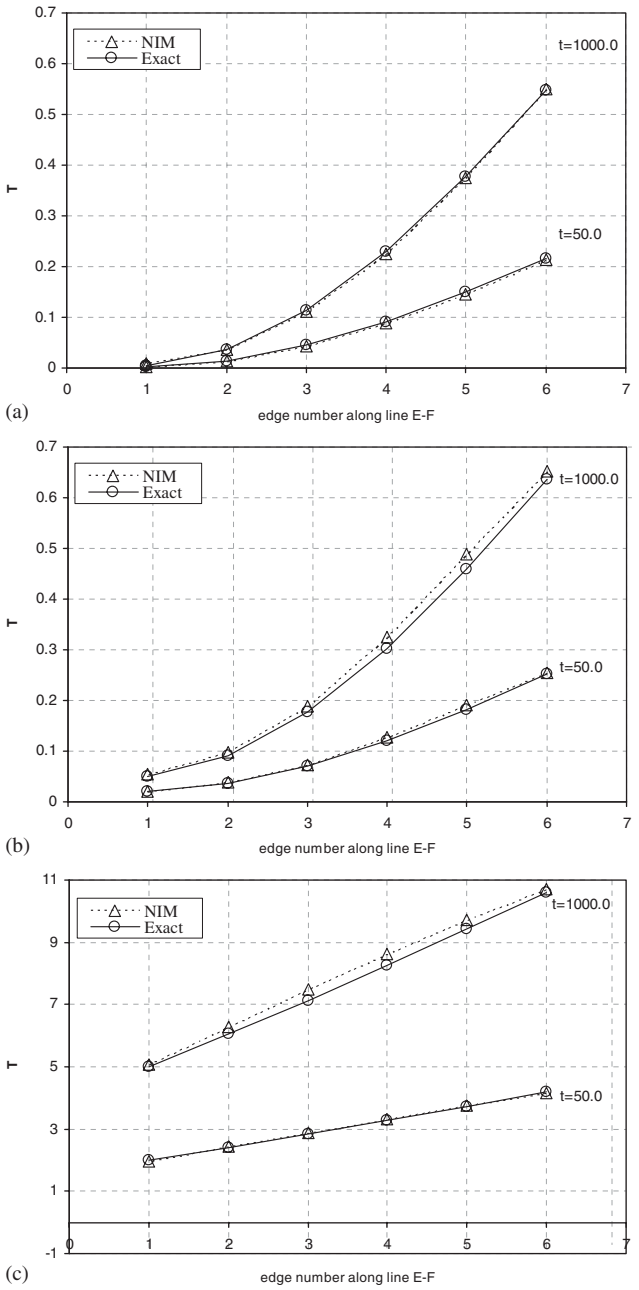

Figure 9. Calculated values for the time-dependent convection–diffusion problem along the *EF* with 6×6 grid. The edge numbers are counted from E to F: (a) $Pe = 700$; (b) $Pe = 70$; and (c) $Pe = 0.7$.

DOI: 10.1002/fld

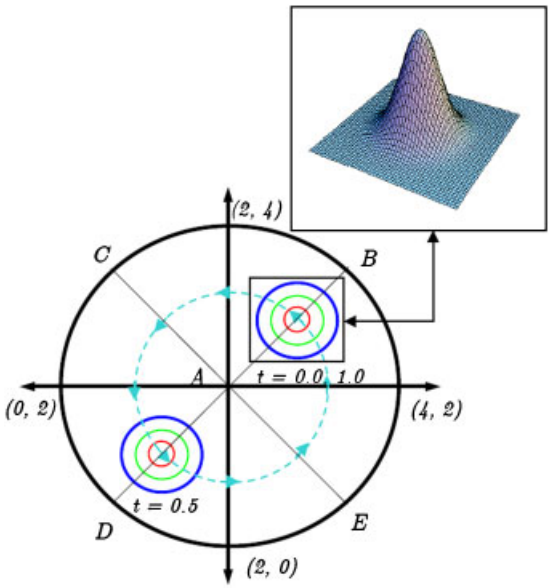

Figure 10. Schematic of the Gaussian hump problem.

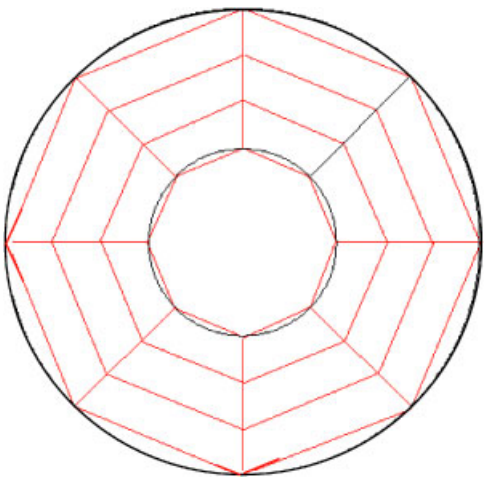

Figure 11. Generic grid for the Gaussian hump problem.

However, the errors do not increase significantly for substantial distortion of the elements. The application of the developed scheme shows that the high accuracy of the NIM is maintained with the transformed equations.

DOI: 10.1002/fld

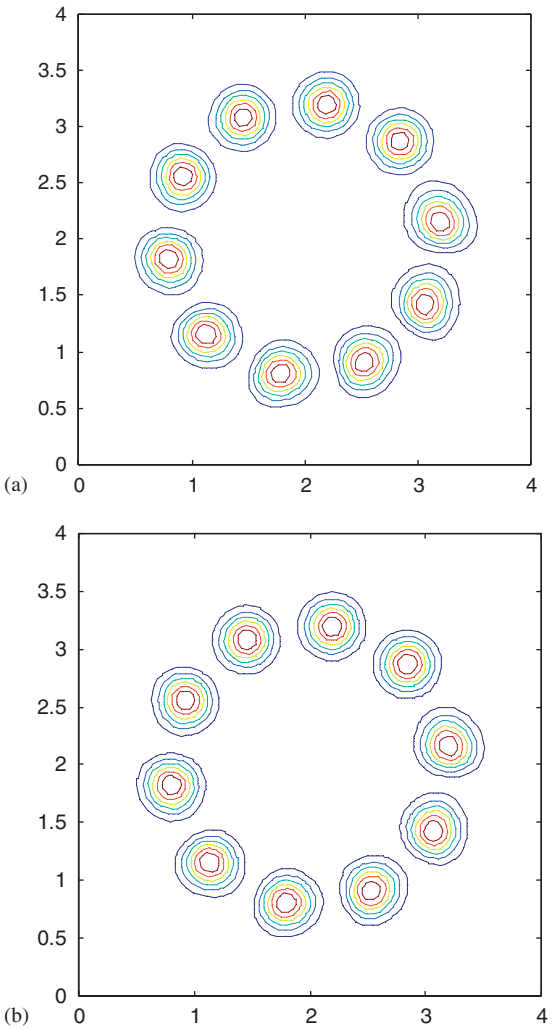

Figure 12. Convection of the Gaussian hump in a rotational flow field with (a) 3600 elements and (b) 4800 elements.

APPENDIX A

For simplicity, Equation (1) can be written as

$$\begin{aligned} x &= C_0 + C_1 s + C_2 t + C_3 st \\ y &= D_0 + D_1 s + D_2 t + D_3 st \end{aligned} \tag{A1}$$

DOI: 10.1002/fld

where

$$\begin{aligned} C_0 &= (x_1+x_2+x_3+x_4)/4 \\ C_1 &= (x_1-x_2-x_3+x_4)/4 \\ C_2 &= (x_1+x_2-x_3-x_4)/4 \\ C_3 &= (x_1-x_2+x_3-x_4)/4 \\ D_0 &= (y_1+y_2+y_3+y_4)/4 \\ D_1 &= (y_1-y_2-y_3+y_4)/4 \\ D_2 &= (y_1+y_2-y_3-y_4)/4 \\ D_3 &= (y_1-y_2+y_3-y_4)/4 \end{aligned} \tag{A2}$$

In Equation (A1) s and t can be thought of as dependent variables written in terms of independent variables x and y (in fact one can solve Equation (A1) for x and y). Hence, in order to transform a typical PDE of the first or second order into local coordinate system, one has to transform respective coefficients into the local coordinate system.

Differentiating Equation (A1) with respect to x gives

$$\begin{aligned} 1 &= C_1 s_x + C_2 t_x + C_3(s_x t + t_x s) \\ 0 &= D_1 s_x + D_2 t_x + D_3(s_x t + t_x s) \end{aligned} \tag{A3}$$

and differentiating the same equation with respect to y

$$\begin{aligned} 0 &= C_1 s_y + C_2 t_y + C_3(s_y t + t_y s) \\ 1 &= D_1 s_y + D_2 t_y + D_3(s_y t + t_y s) \end{aligned} \tag{A4}$$

Combining Equations (A3) and (A4)

$$\begin{bmatrix} C_1+tC_3 & C_2+sC_3 \\ D_1+tD_3 & D_2+sD_3 \end{bmatrix} \begin{bmatrix} s_x & s_y \\ t_x & t_y \end{bmatrix} = \mathbf{I} \tag{A5}$$

or

$$J(x,y) = \begin{bmatrix} s_x & s_y \\ t_x & t_y \end{bmatrix} = \begin{bmatrix} C_1+tC_3 & C_2+sC_3 \\ D_1+tD_3 & D_2+sD_3 \end{bmatrix}^{-1} \tag{A6}$$

This process allows one to obtain $s_x s_y$, etc. in terms of s and t without solving the nonlinear equation.

The same approach can be used for second derivatives as follows. Differentiating Equation (A3) with respect to x yields

$$\begin{aligned} 0 &= C_1 s_{xx} + C_2 t_{xx} + C_3(2s_x t_x + s_{xx} t + t_{xx} s) \\ 0 &= D_1 s_{xx} + D_2 t_{xx} + D_3(2s_x t_x + s_{xx} t + t_{xx} s) \end{aligned} \tag{A7}$$

Differentiating Equation (A4) with respect to y, results in

$$\begin{aligned} 0 &= C_1 s_{yy} + C_2 t_{yy} + C_3(2s_y t_y + s_{yy} t + t_{yy} s) \\ 0 &= D_1 s_{yy} + D_2 t_{yy} + D_3(2s_y t_y + s_{yy} t + t_{yy} s) \end{aligned} \tag{A8}$$

DOI: 10.1002/fld

Equations (A7) and (A8) can be combined to yield

$$\begin{bmatrix} C_1+tC_3 & C_2+sC_3 \\ D_1+tD_3 & D_2+sD_3 \end{bmatrix} \begin{bmatrix} s_{xx} & s_{yy} \\ t_{xx} & t_{yy} \end{bmatrix} = -2 \begin{bmatrix} C_3 s_x t_x & C_3 s_y t_y \\ D_3 s_x t_x & D_3 s_y t_y \end{bmatrix} \tag{A9}$$

or

$$\begin{bmatrix} s_{xx} & s_{yy} \\ t_{xx} & t_{yy} \end{bmatrix} = -2 \begin{bmatrix} C_1+tC_3 & C_2+sC_3 \\ D_1+tD_3 & D_2+sD_3 \end{bmatrix}^{-1} \begin{bmatrix} C_3 s_x t_x & C_3 s_y t_y \\ D_3 s_x t_x & D_3 s_y t_y \end{bmatrix} \tag{A10}$$

or

$$\begin{bmatrix} s_{xx} & s_{yy} \\ t_{xx} & t_{yy} \end{bmatrix} = -2J(x, y) \begin{bmatrix} C_3 s_x t_x & C_3 s_y t_y \\ D_3 s_x t_x & D_3 s_y t_y \end{bmatrix} \tag{A11}$$

APPENDIX B

Operating the original PDE (Equation (9)) by $\frac{1}{4}\int_{-1}^{1}\int_{-1}^{1} \mathrm{d}s\,\mathrm{d}t$ and invoking the definitions of pseudo-source terms yields

$$S_1^{s0} + S_2^{t0} + \frac{1}{4}\int_{-1}^{1}\int_{-1}^{1} f_5 T_{st}\,\mathrm{d}s\,\mathrm{d}t = \bar{p}^{st} \tag{B1}$$

However,

$$\begin{aligned} \frac{1}{4}\int_{-1}^{1}\int_{-1}^{1} f_5 T_{st}\,\mathrm{d}s\,\mathrm{d}t &\approx \frac{1}{4} f_{50} \int_{-1}^{1}\int_{-1}^{1} T_{st}\,\mathrm{d}s\,\mathrm{d}t \\ &= f_{50}\frac{T(1,1)-T(-1,1)-T(1,-1)+T(-1,-1)}{4} \end{aligned} \tag{B2}$$

Approximating

$$T(1,1)-T(-1,1)-T(1,-1)+T(-1,-1) \approx 0 \tag{B3}$$

This assumption yields Equation (15).

DOI: 10.1002/fld

APPENDIX C

The integrals in Equation (18) are evaluated as follows:

$$
\begin{aligned}
f_{10}=0 \quad & \frac{1}{2}\int_{-1}^{1}\bar{T}^t\,\mathrm{d}s = -\frac{C_2}{3f_{30}}+\frac{\bar{T}^t(1)+\bar{T}^t(-1)}{2} \\
f_{10}\neq 0 \quad & \frac{1}{2}\int_{-1}^{1}\bar{T}^t\,\mathrm{d}s = \frac{-C_2}{f_{10}}+\frac{C_2}{f_{30}}-\frac{2C_2/f_{10}}{\exp\left(2\dfrac{f_1}{f_3}\right)-1} \\
& \qquad -\frac{f_3}{f_1}\left(\frac{\bar{T}^t(1)-\bar{T}^t(-1)}{2}\right) \\
& \qquad +\frac{\bar{T}^t(1)\exp\left(2\dfrac{f_1}{f_3}\right)-\bar{T}^t(-1)}{\exp\left(2\dfrac{f_1}{f_3}\right)-1}
\end{aligned}
\tag{C1}
$$

$$
\begin{aligned}
f_{20}=0 \quad & \frac{1}{2}\int_{-1}^{1}\bar{T}^s\mathrm{d}t = -\frac{C_1}{3f_{40}}+\frac{\bar{u}^s(1)+\bar{u}^s(-1)}{2} \\
f_{20}\neq 0 \quad & \frac{1}{2}\int_{-1}^{1}\bar{T}^s\mathrm{d}t = \frac{-C_1}{f_{20}}+\frac{C_1}{f_{40}}-\frac{2C_1/f_{20}}{\exp\left(2\dfrac{f_2}{f_4}\right)-1} \\
& \qquad -\frac{f_4}{f_2}\left(\frac{\bar{T}^s(1)-\bar{T}^s(-1)}{2}\right) \\
& \qquad +\frac{\bar{T}^s(1)\exp\left(2\dfrac{f_2}{f_4}\right)-\bar{T}^s(-1)}{\exp\left(2\dfrac{f_2}{f_4}\right)-1}
\end{aligned}
\tag{C2}
$$

REFERENCES

1. Lawrence RD. Progress in nodal methods for the solutions of the neutron diffusion and transport equations. *Progress in Nuclear Energy* 1986; **17**(3):271–301.
2. Elnawawy OA, Valocchi AJ, Ougouag AM. The cell analytical–numerical method for solution of the advection–dispersion equation: two-dimensional problems. *Water Resources Research* 1990; **26**(11):2705–2716.
3. Horak WC, Dorning JJ. A nodal coarse-mesh method for the efficient numerical solution of laminar flow problems. *Journal of Computational Physics* 1985; **59**:405–440.
4. Wescott B, Rizwan-uddin. An efficient formulation of the modified nodal integral method and application to the two dimensional Burgers equation. *Nuclear Science and Engineering* 2001; **139**:293–305.
5. Hennart JP. A general family of nodal schemes. *SIAM Journal on Scientific and Statistical Computing* 1986; **7**(1):264–287.
6. Azmy YY, Dorning JJ. A nodal integral approach to the numerical solution of partial differential equations. *Advances in Reactor Computations* 1983; **II**:893–909.
7. Wilson GL, Rydin RA, Azmy YY. Time-dependent nodal integral method for the investigation of bifurcation and nonlinear phenomena in fluid flow and natural convection. *Nuclear Science and Engineering* 1988; **100**:414–425.

DOI: 10.1002/fld

8. Azmy YY. Nodal method for problems in fluid mechanics and neutron transport. *Ph.D. Thesis*, University of Illinois, 1985.
9. Esser PD, Witt RJ. An upwind nodal integral method for incompressible fluid flow. *Nuclear Science and Engineering* 1993; **114**:20–35.
10. Michael EPE, Dorning JJ, Rizwan-uddin. Studies on nodal integral methods for the convection–diffusion heat equation. *Nuclear Science and Engineering* 2001; **137**:380–399.
11. Wang F, Rizwan-uddin. A modified nodal scheme for the time-dependent, incompressible Navier–Stokes equations. *Journal of Computational Physics* 2003; **187**:168–196.
12. Wang F, Rizwan-uddin. Modified nodal integral method for the three-dimensional time-dependent incompressible Navier–Stokes equations. *Nuclear Science and Engineering* 2005; **149**:107–114.
13. Toreja AJ, Rizwan-uddin. Hybrid numerical methods for convection–diffusion problems in arbitrary geometries. *Computers and Fluids* 2003; **32**(6):835–872.
14. Gu Y, Rizwan-uddin. A hybrid method for multi-group neutron diffusion equations in arbitrary geometry. *International Topical Meeting on Mathematics and Computations*, *Supercomputing*, *Reactor Physics and Nuclear and Biological Applications*, Avignon, France, 2005. On CD ROM.
15. Zienkiewicz OC, Taylor RL. *The Finite Element Method*, *Volume 1*, *The Basis.* Butterworth: Hienmann, MA, 2000.
16. Barlow J. More on optimal stress points—reduced integration, element distortion and error estimation. *International Journal for Numerical Methods in Engineering* 1989; **28**:1487–1504.
17. Boerner EFI, Loehnert S, Wriggers P. A new finite element based on the theory of a Cosserat point—extension to initially distorted elements for 2D plane strain. *International Journal for Numerical Methods in Engineering* 2007; **71**:454–472.
18. Chen XM, Cen S, Long YQ, Yao ZH. Membrane elements insensitive to distortion using the quadrilateral area coordinate method. *Computers and Structures* 2004; **82**:35–54.
19. Rajendran S, Liew KM. A novel unsymmetric 8-node plane element immune to mesh distortion under a quadratic displacement field. *International Journal for Numerical Methods in Engineering* 2003; **58**:1713–1748.
20. Rajendran S, Liew KM, Wang W. A quadratic plane triangular element immune to quadratic mesh distortions under quadratic displacement fields. *Computer Methods in Applied Mechanics and Engineering* 2006; **195**:1207–1223.
21. Prathap G, Senthilkumar V, Manju S. Mesh distortion immunity of finite elements and the best-fit paradigm. *Sadhana* 2006; **31**:505–514.
22. Cen S, Chen XM, Fu XR. Quadrilateral membrane element family formulated by the quadrilateral area coordinate method. *Computer Methods in Applied Mechanics and Engineering* 2007; **196**:4337–4353.
23. Ooi ET, Rajendran S, Yeo JH. A 20-node hexahedron element with enhanced distortion tolerance. *International Journal for Numerical Methods in Engineering* 2004; **60**:2501–2530.
24. Rajendran S, Ooi ET, Yeo JH. Iterative correction to enhance the mesh distortion tolerance of isoparametric QUAD8 element. *Communications in Numerical Methods in Engineering* 2005; **21**:457–464.
25. Faghri M, Sparrow EM, Prata AT. Finite-difference solutions of convection–diffusion problems in irregular domains, using a nonorthogonal coordinate transformation. *Numerical Heat Transfer* 1984; **7**:183–209.

DOI: 10.1002/fld